Proceedings of the 11th World Congress on New Technologies (NewTech'25)
Paris, France - August, 2025
Paper No. ICNFA 130
DOI: 10.11159/icnfa25.130

Development of an Autonomous Battery Charging System for Micro Aerial Vehicles via Nanoantenna Based Energy Harvesting Mechanism

Chayanika Baishya[1], Amarnath Kumar[1], Sisir Kumar Nayak[1], Harshal B. Nemade[1]
[1]Indian Institute of Technology, Guwahati
Guwahati, Assam, India
cbaishya@iitg.ac.in, amarnathkumar@iitg.ac.in, sknayak@iitg.ac.in, harshal@iitg.ac.in

Abstract – This study proposes the design and simulation of a nanorectenna-based energy harvesting system for the autonomous charging of Micro Air Vehicle (MAV) batteries. An arrow pentagon-shaped nanoantenna is developed to efficiently capture infrared (IR) radiation from the environment which resonates at 28.3 THz frequency. The harvested IR energy is converted into direct current (DC) using a metal-insulator-metal (MIM) diode. A numerical analysis of the MIM diode is conducted to extract key electrical parameters. The feasibility of MAV battery charging is demonstrated using these parameters and array calculations. Since IR radiation is always present in the environment, the results highlight the strong potential of the proposed nanorectenna system to enable sustainable, in-flight battery charging for MAVs, regardless of time or location.

Keywords**:** Micro Aerial Vehicle (MAV), Arrow Pentagonal Nanoantenna, Metal-Insulator-Metal (MIM) diode, Electromagnetic (EM), Wireless Power Transfer (WPT)

1. Introduction

Unmanned Aerial Vehicles (UAVs), often referred to as the eyes and ears beyond enemy lines, have become increasingly significant in modern society due to their payload-carrying capabilities and compact form factors. These systems are capable of operating in complex environments without the need for onboard human pilots. Presently, UAVs are employed across a wide range of applications, including military operations, power line surveillance, forest monitoring, disaster management, and precision agriculture. Typically, these UAVs are powered by high-capacity energy sources such as lithium-based batteries, which enable flight durations of approximately 20-40 minutes [1].

With advances in electronic miniaturization and integration, a novel category of UAVs known as Micro Aerial Vehicles (MAVs) has emerged. These hand-launched aerial platforms, weighing less than 100 grams, are designed to operate in environments that are inaccessible or hazardous to larger UAVs. MAVs are characterized by their lightweight, portable, and rapidly deployable nature. They are capable of transmitting real-time data, such as live video feeds to ground stations, and are optimized for quick assembly and disassembly during field operations [2].

Despite their many advantages, MAVs face significant technological limitations, particularly in terms of flight time, which is directly constrained by the onboard battery capacity. This limitation restricts mission duration and operational range, as their performance is heavily dependent on energy availability [2]. These systems typically rely on lithium-based batteries due to their high energy density and lightweight nature [1]. lithium-polymer (Li-Po) batteries are especially favored for their high discharge rates and flexibility in design [3]. Currently, batteries power over 96% of commercial and personal UAVs. However, their effectiveness declines in missions where recharging is not feasible, highlighting the need for more efficient and sustainable energy solutions [2].

To extend flight duration, two main strategies can be considered: increasing battery capacity or enabling in-situ battery charging. However, due to current battery technology limitations, achieving a balance between energy storage and system weight remains challenging. Enhancing battery capacity often results in additional weight, which adversely affects overall performance. An alternative is to adopt wired or wireless charging methods. Wireless charging, in particular, offers significant advantages by eliminating the need for UAVs to return to base, thereby improving operational flexibility. Additionally, it removes the requirement for physical charging ports, making MAVs more suitable for enclosed designs and harsh weather conditions such as rain or snow [3].

Several power and charging technologies have been explored in the literature, including battery-powered systems, battery swapping, dynamic soaring, tethered UAVs, charging from power lines, fuel cells, supercapacitors, photovoltaic cells, far-field wireless power transfer (WPT) methods like laser and distributed laser charging [1] and near-field technologies like

inductive power transfer (IPT) and capacitive power transfer (CPT) [4]. Nevertheless, wireless power systems present their own challenges, such as limited efficiency, alignment issues, added system weight due to transmission and receiver coils, complex control strategies, and potential electromagnetic (EM) interference affecting human safety [3].

An effective approach to address current energy limitations in MAVs is environmental energy harvesting. This method enables the development of highly efficient, self-powered systems capable of providing a continuous energy supply [5]. Among available sources, infrared (IR) radiation is particularly promising, as it constitutes nearly half of the solar spectrum reaching Earth. IR radiation not only originates from solar energy but is also present as waste heat from processes such as metal heating, fluid heating, and steam generation. This energy spans temperatures between 400 and 2000 K and corresponds to mid-IR wavelengths ranging from 2 to 11 μm, with peak intensity at 10.8 μm (28.3 THz) [6]. The concept involves capturing IR radiation as high-frequency EM waves using a rectenna, which is a combination of a nanoantenna and a diode. When subjected to IR sources, nanoantennas generate strong localized electric fields through surface plasmon resonance, especially at the antenna arms. Converting these localized THz waves into usable DC signals is a technical challenge, addressed using metal-insulator-metal (MIM) tunneling diodes [7]. This technique utilizes plasmonic rectennas that absorb incident IR radiation and convert the induced alternating current (AC) into DC, thereby charging the onboard battery. The antennas function based on natural resonance to maximize energy capture [5]. Fig. 1 shows the schematic of a nanorectenna setup.

In this study, the design and simulation of an arrow-shaped pentagon nanoantenna resonating at 28.3 THz is presented. The AC voltage induced within the antenna gap is rectified using a MIM diode, with numerical modeling performed based on Simmons' formula. The diode parameters are subsequently extracted for further analysis. Finally, the DC voltage output required to charge the MAV battery is calculated, and the total number of nanoantennas needed in a series-parallel configuration is determined using antenna array calculations.

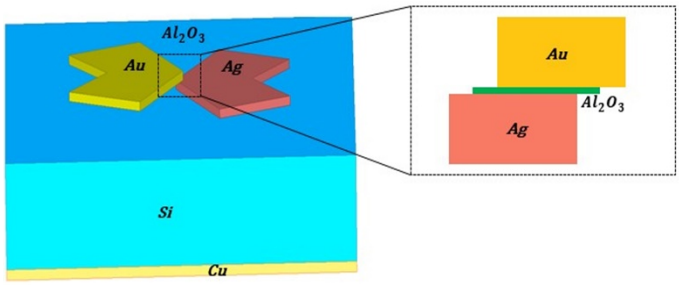

Fig. 1: Schematic of a nanorectenna setup.

2. Rectenna Design

2.1. Design and Simulation of Nanoantenna

The pentagonal nanoantenna was designed using CST Microwave Studio software. The substrate consists of a 1.15 μm thick silicon layer, with a 115 nm thick copper film working as a backplane at the bottom of the antenna. The antenna consists of gold (Au) and silver (Ag) arms with a finite gap and height of 100 nm.

Perfectly matched layers (PML) are used as absorbing boundary conditions for removing artificial reflections. The EM fields in the nanoantenna gap are characterized using a Cartesian coordinate system, with the x- and y-axes located in the antenna plane and the z-axis oriented perpendicular to this plane. The EM field in the nanoantenna gap is calculated based on the assumption of plane wave illumination having a magnitude of 1 V/m, with polarization directed along the antenna axis.

The side length of the pentagonal antenna (L) can be determined by inscribing it within a circle of radius (r). The relation between L and r is defined accordingly.

$$L = 2r\sin\left(\frac{\pi}{5}\right) \tag{1}$$

The resonant frequencies, including those of the dominant mode and higher-order modes, can be determined using the formula provided [8].

$$f_{np} = \frac{X_{np}^{'} c}{2\pi r\sqrt{\epsilon_r}} \tag{2}$$

Where, $X_{np}^{'}$ are the zeros of the derivative of the Bessel function $J_n(x)$ of the order n, as is true for TE mode, however for the lowest order modes, $X_{np}^{'}$= 1.84118. c is the velocity of light and ϵ_r is permittivity of the substrate material.

Nanoantenna structures exhibit significant sensitivity to their geometric arrangement. Parameters including shape, size, aspect ratio, and spatial arrangement are crucial in determining their resonance characteristics, field enhancement abilities, and spectral performance. In this paper, the arrow pentagon structure is designed with a rear-side cut angle of 62.5° while maintaining the original dimensions of the other sides.

2.2. Analysis and Formulation of Field Enhancement in an Array

According to reference [9] , in a serial array of antennas, the field intensity in the array gap is given by:

$$E_{Total} = E_{single\ element\ at\ reference\ point} \times AF \tag{3}$$

in which, AF is the Array Factor, which is defined as:

$$AF = \sum_{n=1}^{N=1} e^{j(n-1)\psi}, \ \psi = kd\cos\theta + \beta \tag{4}$$

In equation (4), N denotes the total number of array elements (i.e., antennas), k represents the wave number defined as $2\pi/\lambda$, d is the spacing between the elements, θ is the angle between the array axis and the incident plane wave vector, and β is the phase shift between adjacent elements. In the proposed serial array configuration, the incident wave impinges perpendicularly on the antenna surface, resulting in θ being 90°. Additionally, the signals received by all antenna elements are assumed to be in phase, enabling constructive interference, provided the interconnecting metal lines are of appropriate length. Consequently, the phase shift β is zero. Under these conditions, ψ becomes zero, leading to a simplified form of equation (5).

$$E_{Total} = E_{single\ element} \times N \tag{5}$$

In the above equations, the losses associated with the extensive network of interconnecting metal lines are not considered. When these losses are considered, field intensity with respect to the number of elements (N) is not directly proportional. Consequently, the field intensity scales with to N^{α}, in which, $\alpha < 1$. Hence, the field enhancement within the array gap can be approximated using the following expressions:

$$E_s = E_1 \times (N_s)^{\alpha_s} \tag{6}$$

$$E_p = E_1 \times (N_s)^{\alpha_p} \tag{7}$$

Here, E_1 denotes the field enhancement within the gap of a single-element antenna, while E_S and E_P represent the field enhancements for array configurations in series and parallel, respectively. The parameters N_S and N_P correspond to the number of array elements in the series and parallel configurations. Additionally, α_S and α_P are scaling factors with values close to unity, adopted from [9] as 0.96 and 0.83, respectively.

The proposed configuration consists of a combinational structure comprising $N_S \times N_P$ array elements, where N_S denotes the number of elements connected in series within each array, and N_P represents the number of such series arrays connected in parallel. The total electric field enhancement for this combinational array structure can be estimated as follows:

$$E_{Total} = E_s \times (N_p - array)^{\alpha_p} \tag{8}$$

$$E_{Total} = E_1 \times (N_s)^{\alpha_s} \times (N_p - array)^{\alpha_p} \tag{9}$$

2.3. Design of MIM Diode

The performance of tunnel diodes is characterized by several key parameters: (1) differential or dynamic resistance (R_d), (2) responsivity (M), (3) nonlinearity (NL), and (4) cut-off frequency (f_c). The differential resistance (R_d) is defined as the derivative of the current (I) with respect to the applied voltage (V_b), as expressed in equation (10). For efficient impedance matching between the diode and the antenna, it is crucial that R_d remains low.

$$R_d = \frac{dV}{dI} \tag{10}$$

The second critical parameter is the diode responsivity, which serves as an indicator of the diode's tunneling efficiency. This parameter can be mathematically defined as follows:

$$M = \frac{\frac{d^2I}{dV^2}}{\frac{dI}{dV}} \tag{11}$$

Diode responsivity is a critical parameter that quantifies the efficiency of converting AC signals into DC. A higher responsivity indicates a superior rectification performance of the diode. Additionally, diode nonlinearity is an important characteristic, typically described using the nonlinear factor, which reflects the extent of deviation from linear behavior in the diode's current-voltage response.

$$NL = \frac{d^2I}{dV^2} \tag{12}$$

The last parameter, diode cutoff frequency is expressed as follows:

$$f_c = \frac{1}{2\pi R_d C} \tag{13}$$

$$C = \varepsilon_0 \varepsilon_r \frac{A}{d} \tag{14}$$

Here, R_d represents the equivalent resistance of both the diode and the antenna, while C denotes the capacitance of the diode. ε_0 and ε_r correspond to the vacuum permittivity and the relative permittivity of the oxide material, respectively. A is the junction or overlap area of the oxide layer within the diode, and d denotes the thickness of the oxide layer. For aluminium oxide (Al_2O_3), ε_r is taken as 0.304. In this analysis, the junction area is assumed to be 100 nm², and the oxide thickness is considered to be 1 nm to ensure efficient tunneling [7].

With the electrode of higher work function negatively biased, there is a net flow of electrons from this electrode to the electrode of lower function. In this configuration, the externally applied field aligned with the internal electric field of the diode, resulting in an overall enhancement of the net electric field. This is explained with the help of the band diagram in Fig. 2. Gold (Au) and silver (Ag) are employed as the metal components of the nanoantenna arms, with their respective work functions reported as 5.1 eV and 4.26 eV [10] . The significant difference in work function between these metals is strategically utilized to promote efficient electron tunneling [11]. Al_2O_3 was selected as the insulating material due to its low dielectric constant at THz frequencies, enabling optimal alignment with the operational cut-off frequency of 28.3 THz for enhanced absorption of incident IR radiation [10].

The current density J in a tunnel junction comprising dissimilar electrodes is mathematically expressed as a function of the applied bias voltage (V_b), as given by the following equation: [12]

$$J = J_0\left\{\bar{\varphi}\exp\left(-A\sqrt{\bar{\varphi}}\right) - \left(\bar{\varphi} + eV_b\right)\exp\left(-A\sqrt{\bar{\varphi} + eV_b}\right)\right\} \tag{15}$$

$$A = \frac{4\pi\Delta s\sqrt{2m}}{h}, \quad J_0 = \frac{e}{2\pi h(\Delta s)^2}$$

Where e is the electric charge of the electron, m is the mass of the electron, h is the Planck's constant, V_b is the applied bias, $\bar{\varphi}$ is the mean barrier height, Δs = s2-s1, where s1 and s2 are limits of barrier at Fermi level. s is the tunnel barrier thickness, and J is the tunneling current density. The $\bar{\varphi}$ can be expressed as:

$$\bar{\varphi} = \frac{1}{\Delta s}\int_{s1}^{s2}\left[\varphi_2 - \left(\Delta\varphi + eV_b\right)\left(\frac{x}{s}\right) - \frac{1.15\lambda s^2}{x(s-x)}\right]dx \tag{16}$$

$$s1 = \frac{1.2\lambda s}{\varphi_2} \tag{17}$$

$$s2 = s - \frac{9.2\lambda s}{3\varphi_2 + 4\lambda - 2\left(eV_b + \Delta\varphi\right)} + \frac{1.2\lambda s}{\varphi_2} \tag{18}$$

Where $\Delta\varphi$ is the difference in barrier heights between interfaces of the insulator with the top and bottom electrodes, φ_1 and φ_2 are the barrier heights at the interface of respective electrodes and the insulator, λ is the wavelength. Therefore, the equivalent rectified DC voltage component can be extracted as: [13]

$$V_{rect} = \frac{1}{4}\frac{I''(V_b)}{I'(V_b)}V_{ac}^2 \tag{19}$$

Here, I′ is the first derivative of the tunneling current, and I″ is the second derivative of the tunneling current.

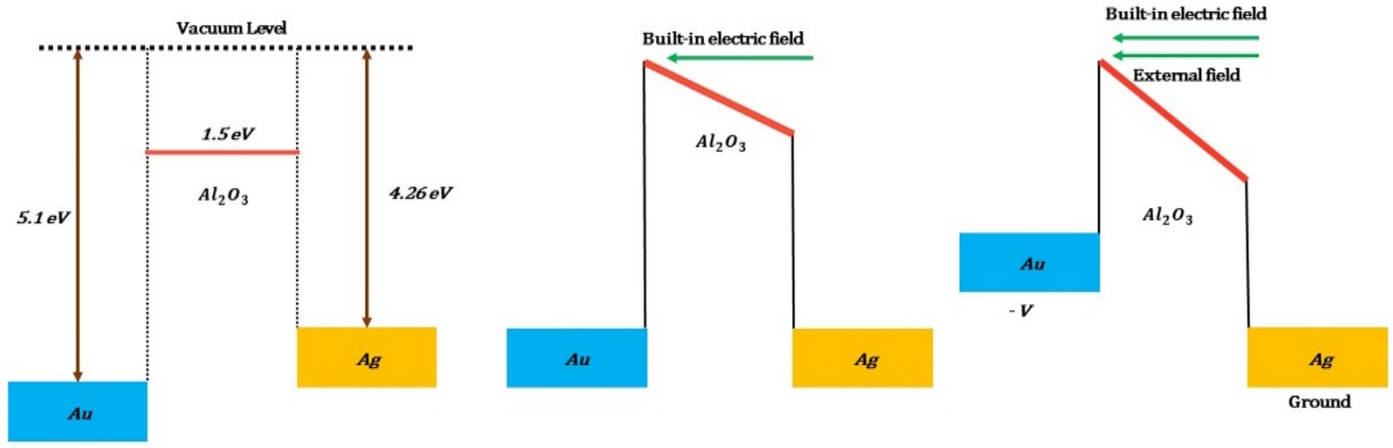

Fig. 2: Band diagram of MIM diode.

2.4. MAV Battery Specification

Energy harvesting (EH) systems inherently exhibit intermittent behavior, resulting in voltage and current output fluctuations. In contrast, batteries provide a stable and consistent power supply to the load. For EH applications, integrating rechargeable batteries is essential to ensure reliability and continuity of power. In current MAV designs, batteries serve as the primary energy source for all onboard components, including electronic circuits, sensors, actuators, and communication modules. The battery's capacity and energy density influence overall flight duration [4].

This study employs a rechargeable Li-Po battery with a nominal voltage of 3.7 V and a capacity of 90 mAh, selected based on the trade-off between energy storage and physical size. The battery weighs approximately 1.5 grams. To enhance mission capability, it is necessary to ensure that, at any given time, the available energy meets or exceeds the energy demand of the system [2].

3. Results and Discussion

The electric field concentrated in the gap of the arrow pentagon structure is shown in Fig. 3(a). It is seen that a maximum field of 53.88 V/m is concentrated in the gap region when it is radiated with a field of 1 v/m. The reflection and impedance parameters of the antenna are shown in Fig. 3(b) and 3(c). The antenna has a magnitude of $S_{11,}$ approximately equal to -35 dB at 28.3 THz. The structures exhibit the real part of the impedance value close to that of free space (approximately 377 Ω), and the imaginary part is very small. Therefore, from the simulation result of the nanoantenna, it can be concluded that the antenna has a high enhancement capability with a minimum reflection coefficient and good impedance matching with the free space impedance value. Thus, it is suitable for EH applications.

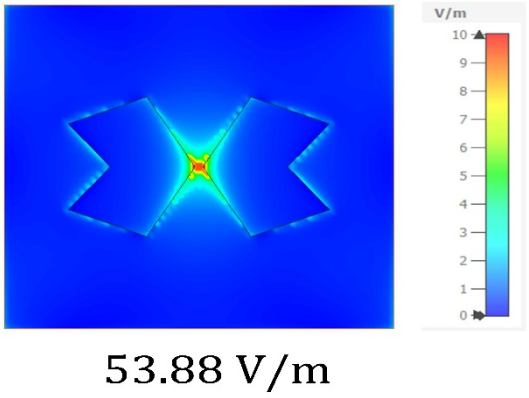

Fig. 3(a): E-field inside arrow pentagon nanoantenna.

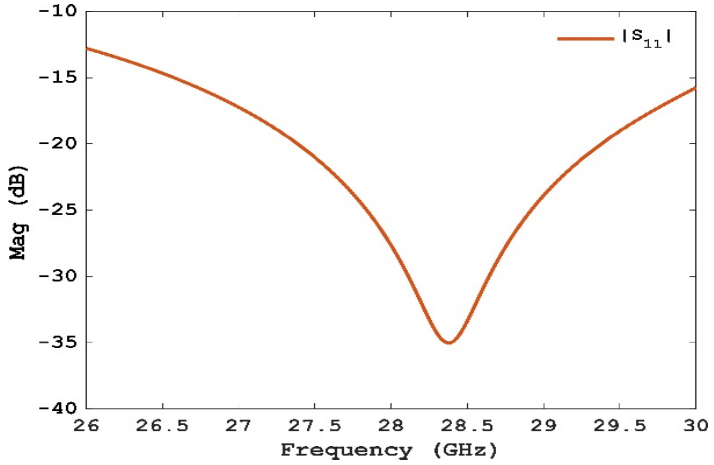

Fig. 3(b): S_{11} parameter of the arrow pentagon nanoantenna at 28.3 THz

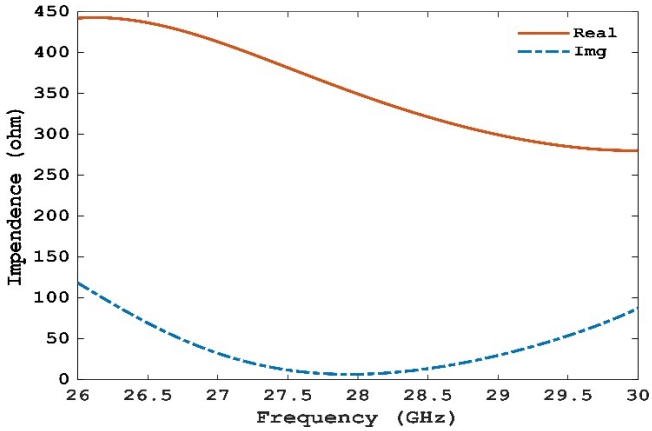

Z_{11} (Re) = 332.02 Ω

Z_{11} (Im) = 9.55 Ω

Fig. 3(c): Z_{11} parameter of the arrow pentagon nanoantenna at 28.3 THz

The |J|-V and I-V characteristics of the MIM diode are illustrated in Fig. 4(a) and Fig. 4(b), respectively. From the I-V data, key performance parameters, including dynamic resistance, nonlinearity, and responsivity, were extracted using equations (10)-(12). As the study primarily aims to evaluate zero-bias performance, particular emphasis was placed on determining responsivity and dynamic resistance at zero bias, as depicted in Fig. 4(a)-(c). It was observed that both the I-V behavior and responsivity exhibited high sensitivity to variations in the oxide layer thickness. Additionally, nonlinearity was found to be strongly correlated with the diode's responsivity; greater nonlinearity resulted in enhanced responsivity. Therefore, MIM diodes exhibiting high responsivity demonstrate superior rectification and tunneling performance.

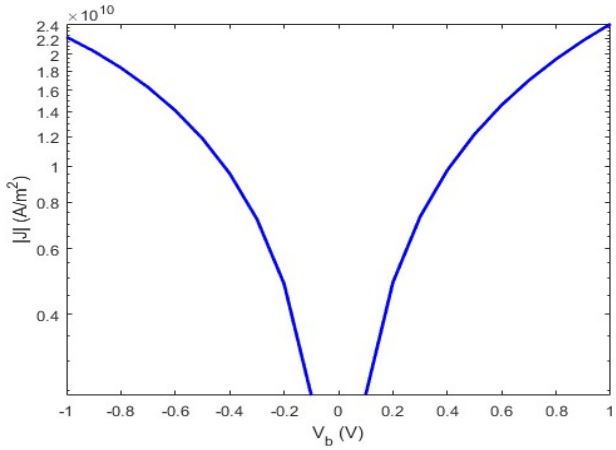

Fig. 4(a): Absolute current density |J| vs V_b

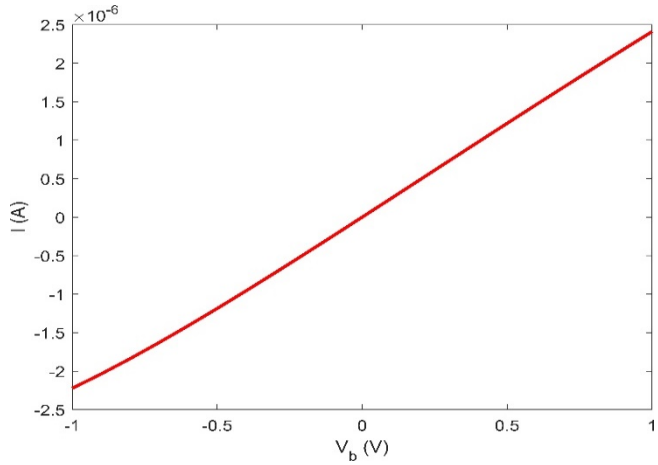

Fig. 4(b): Current I vs V_b

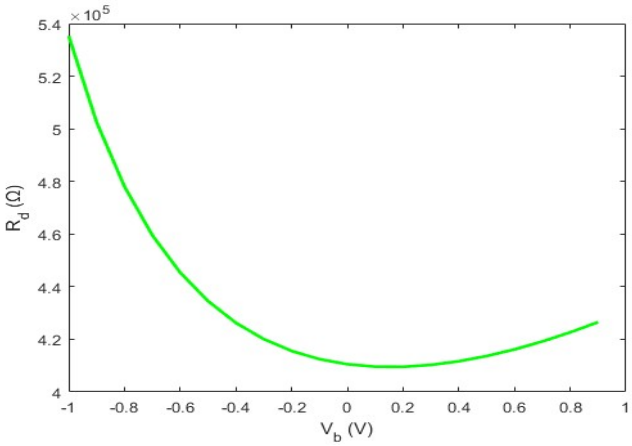

Fig. 4(c): Dynamic resistance R_d vs V_b

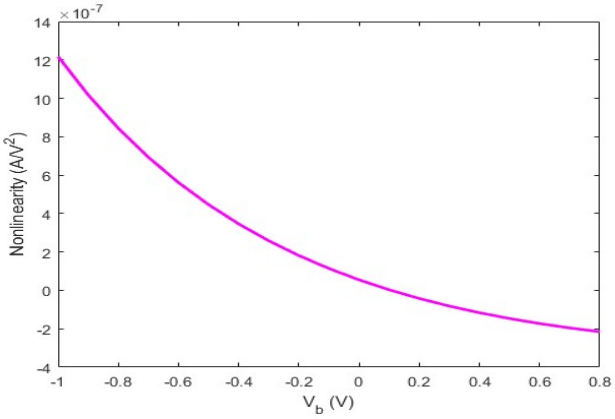

Fig. 4(d): Nonlinearity vs V_b

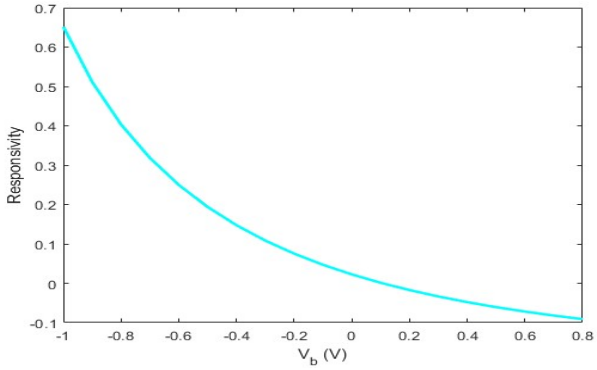

Fig. 4(e): Responsivity vs V_b

As observed in Fig. 4(a), the current density curve exhibits asymmetry, which can be attributed to the use of dissimilar metals on the bottom side of the nanoantenna. At zero bias, the dynamic resistance and responsivity are found to be 410522 Ω and 0.022 A/W, respectively. Considering the charging cut-off voltage of a 3.7 V battery is 4.2 V, the rectified voltage V_{rect} from a single antenna can be estimated using equation (19). Subsequently, equation (9) is employed to determine the

number of antenna elements required to achieve the desired output voltage. Based on this analysis, an array consisting of 3900 × 3900 elements is necessary to charge the MAV battery.

4. Conclusion

This study presents a numerical investigation into autonomous and sustainable battery charging for an MAV. A nanoantenna integrated with a MIM diode is employed as the energy harvesting mechanism. The nanoantenna array is designed to capture IR radiation from the surrounding environment and convert it into DC electrical output through the rectification process facilitated by the MIM diode. The electrical characteristics of the diode are analyzed using Simmons' tunneling model. A numerical calculation is conducted to evaluate the feasibility of charging a 3.7 V Li-Po battery using the nanorectenna system. Results indicate that an array comprising 3900 × 3900 nanoantennas is required for effective charging. The proposed energy harvester is capable of enabling continuous and in-flight battery charging for MAVs, independent of location or time.

Acknowledgments

The IMPRINT-2 initiative by DST, India, and MoE, Govt. of India, supported the research under the project number: IMP/2018/001179.

References

[1] S. A. H. Mohsan, N. Q. H. Othman, M. A. Khan, H. Amjad, and J. Żywiołek, “A Comprehensive Review of Micro UAV Charging Techniques,” *Micromachines*, vol. 13, no. 6, pp. 1–30, 2022.

[2] R. Citroni, F. Di Paolo, and P. Livreri, “A novel energy harvester for powering small UAVs: Performance analysis, model validation and flight results,” *Sensors*, vol. 19, no. 8, pp. 5–10, 2019.

[3] P. K. Chittoor, B. Chokkalingam, and L. Mihet-Popa, “A Review on UAV Wireless Charging: Fundamentals, Applications, Charging Techniques and Standards,” *IEEE Access*, vol. 9, pp. 69235–69266, 2021.

[4] X. Mou, D. Gladwin, J. Jiang, K. Li, and Z. Yang, “Near-Field Wireless Power Transfer Technology for Unmanned Aerial Vehicles: A Systematical Review,” *IEEE J. Emerg. Sel. Top. Ind. Electron.*, vol. 4, no. 1, pp. 147–158, 2022.

[5] R. Citroni, A. Leggieri, D. Passi, F. Di Paolo, and A. Di Carlo, “Nano energy harvesting with plasmonic nano-antennas: A review of MID-IR rectenna and application,” *Adv. Electromagn.*, vol. 6, no. 2, pp. 1–13, 2017.

[6] A. Y. Elsharabasy, A. S. Negm, M. H. Bakr, and M. Jamal Deen, “Global Optimization of Rectennas for IR Energy Harvesting at 10.6 μm,” *IEEE J. Photovoltaics*, vol. 9, no. 5, pp. 1232–1239, 2019.

[7] A. Alodhayb, A. Meredov, and P. Dawar, “A simulation study of multi-junction insulator tunnel diode for solar energy harvesting applications,” *Mater. Res. Express*, vol. 8, no. 9, 2021.

[8] D. Yadav, S. Deshpande, M. Mathpati, D. Atkale, and M. Bakhar, “A Wideband Pentagonal Patch Antenna with Rectangular Slots for Wireless Applications,” *SSRN Electron. J.*, 2020.

[9] A. Chekini, S. Sheikhaei, and M. Neshat, “An infrared energy harvesting device using planar cross bowtie nanoantenna arrays and diode-less rectification based on electron field emission,” *J. Mod. Opt.*, vol. 67, no. 16, pp. 1348–1364, 2020

[10] A. Yahyaoui, A. Elsharabasy, J. Yousaf, and H. Rmili, "Numerical analysis of MIM-based log-spiral rectennas for efficient infrared energy harvesting,” *Sensors*, vol. 20, no. 24, pp. 1–16, Dec. 2020.

[11] G. Jayaswal, A. Belkadi, A. Meredov, B. Pelz, G. Moddel, and A. Shamim, “Optical rectification through an Al2O3 based MIM passive rectenna at 28.3 THz,” *Mater. Today Energy*, vol. 7, pp. 1–9, 2018.

[12] J. G. Simmons, “Electric Tunnel Effect between Dissimilar Electrodes Separated by a Thin Insulating Film,” *J. Appl. Phys.*, vol. 34, no. 9, pp. 2581–2590, 1963.

[13] M. Dagenais, K. Choi, F. Yesilkoy, A. N. Chryssis, and M. C. Peckerar, “Solar spectrum rectification using nano-antennas and tunneling diodes,” in *Optoelectronic Integrated Circuits XII*, SPIE, Feb. 2010, p. 76050E.